PCCP

Accepted Manuscript

ROYAL SOCIETY OF CHEMISTRY

www.rsc.org/pccp

Cite this: DOI: 10.1039/c0xx00000x

www.rsc.org/xxxxxx

ARTICLE TYPE

A Comprehensive Study of Isomerization and Protonation Reactions in the Photocycle of Photoactive Yellow Protein

Lili Wei,[a] Hongjuan Wang,[a] Xuebo Chen,*[a] Weihai Fang[a] and Haobin Wang*[b]

Received (in XXX, XXX) Xth XXXXXXXXX 20XX, Accepted Xth XXXXXXXXX 20XX

DOI: 10.1039/b000000x

Light-activated photoactive yellow protein (PYP) chromopore uses a series of reactions to trigger photo-motility and biological responses, and generate a wide range of structural signalings. To provide a comprehensive mechanism of the overall process at the atomic level, we apply a CASPT2//CASSCF/AMBER QM/MM protocol to investigate the relaxation pathways for a variety of possible isomerization and proton transfer reactions upon photoexcitation of the wild-type PYP. The nonadiabatic relay through an S_1/S_0 conical intersection [$CI(S_1/S_0)$] is found to play decisive major role in bifurcating the excited state relaxation into a complete and a short photocycle. Two major and one minor deactivation channels were found starting from the $CI(S_1/S_0)$-like intermediate I_T, producing the *cis* isomers pR_1, I_{CP}, and I_{CT} through "hula twist", "bicycle pedal" and one-bond flip isomerization reactions. The overall photocycle can be achieved by competitive parallel/sequential reactions, in which the ground state recovery is controlled by a series of slow volume-conserving bicycle pedal/hula twist and one-bond flip isomerization reactions, as well as fast protonation/deprotonation processes and the hydrophobic-hydrophilic state transformation.

Introduction

Photoactive yellow protein (PYP), which was first discovered in the cytoplasm of Halorhodospira halophila bacterium, is a blue light photoreceptor and the structural prototype for the PAS (PER-ARNT-SIM) class of signal transduction proteins.[1-4] The chromopore of PYP absorbs light and converts it to the chemical energy. The process further triggers photo-motility, i.e. photoinduced motion of protein skeletons, which ultimately leads to biological responses based on a wide variety of structural signalings.[5-8] The photocycle process occurs with high efficiency through a multi-step isomerization and proton transfer reaction.[9-11]As a result, very low fluorescence quantum yield ($\Phi=10^{-3}$) was observed for the excited PYP at room temperature.[12]

A protein-labeling technique has been recently developed using a PYP tag, in which the native chromophore of *p*-coumaric acid (*p*CA) is substituted by the thioester derivative of cinnamic acid or coumarin through transthioesterification.[13-16] This alters the electronic structure in the excited state, protein cavity environment, and/or network of the intermolecular hydrogen bonding, and results in a novel fluorogenic probe for no-wash live-cell imaging of proteins fused to the PYP-tag.[14,15] Consequently, the fluorescence quantum yield increases significantly to 0.38~0.47, allowing a rapid detection of proteins in living cells with high signal-to-noise ratio.[14,15] Such a finding indicates that the photocycle mechanism for the isomerization and proton transfer reactions in the wild type (*wt*) PYP has been considerately changed due to the structural modification.

As shown in Figure 1, it is generally accepted that upon blue light excitation *wt*-PYP undergoes a fully reversible photocycle starting from a dark state pG and then going through two early spectroscopic intermediates I_0 and $I^{\ddagger}_0$ [17-20] that maybe equivalent to I_T (an intermediate with a twisted structure) and I_{CP} (an intermediate with a *cis* planar-like structure), respectively.[21,25] Following the initial relaxation, *wt*-PYP decays quickly to a red-

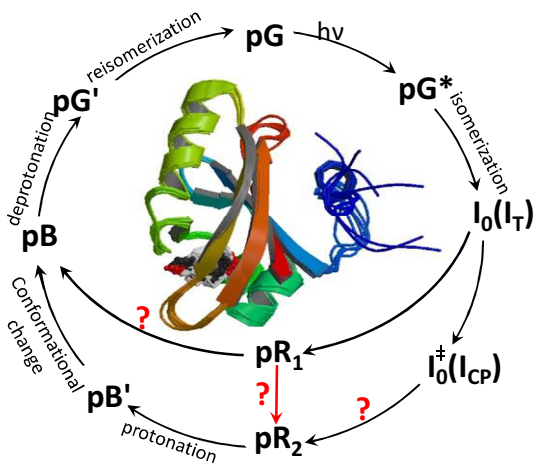

Figure 1: Possible steps and intermediates in the photocycle of PYP. pG: ground state of PYP; pG*: electronically excited state; I_0 and $I^{\ddagger}_0$: ps intermediates, maybe equivalent to I_T and I_{CP} structures; pR: transient red-shifted photocycle intermediate of PYP; pB, transient blue-shifted photocycle intermediate of PYP.

shifted intermediate pR.[22-23] The precise mechanism for generating pR is still unclear. In one proposal, I_T may simultaneously decay to the two intermediates pR_1 and pR_2 (via I_{CP}) through a parallel isomerization reaction.[21,24-26] Another proposed mechanism is that pR_2 is produced after pR_1 via a sequential reaction, i.e. $I_T \rightarrow pR_1 \rightarrow pR_2$.[27-31] In both mechanisms the intermediate pR_2 undergoes a protonation reaction to capture one proton from the Glu46 residue, leading to a blue-shifted intermediate pB'.[32-35] Consequently, an energetically unstable, charged $Glu46^-$ is generated to trigger a large conformational change of the protein, relaxing to a putative signaling state pB which forms a new blue-shifted intermediate.[32-35] Another possibility is that pB may be reached directly from pR_1 because they exhibit similarities in chromophore orientation and surrounding hydrogen-bond networks.[25,26] Eventually the photocycle is completed via a series of deprotonation and re-isomerization processes. A structural recovery of PYP is achieved through a new intermediate pG' with a deprotonated chromophore that facilitates the occurrence of re-isomerization.[36,37]

In the above mechanism identifying all possible intermediates in the photocycle of PYP has posed significant challenges for both experimental and theoretical investigations.[21,25,38-43] There are many open questions, particularly with respect to the much debated parallel versus sequential kinetic pathways, the assignment of various intermediates, and the identity of the donor and acceptor for proton transfer in the multi-step protonation/deprotonation reaction.[44-47] Electronic structure calculations have been done to map out, to a certain extent, the potential energy surface describing atomic motions and relevant reaction dynamics.[48,49] However, to our knowledge previous electronic structure studies mainly focused on the core chromophores of *p*CA[50-54] and did not take into account the protein environment (we note the important work using pure molecular dynamics simulation.[55-60]) Moreover, these studies considered only one or two steps. As a result the energy landscape for the full photocycle of PYP has not been obtained quantitatively, which has limited the understanding of the overall process. From the experimental perspective, although several possible pathways were proposed to address the observed photochemistry based on spectroscopy or X-ray crystallography techniques, it is difficult to reach a definitive conclusion due to the strong overlap in the transient absorption spectra and the lack of information for electron transitions in the crystallographic experiment.

Therefore, it is beneficial to carry out a comprehensive computational study to address the overall process. In this work, a combined quantum mechanical/molecular mechanical (QM/MM) approach, at the level of theory of CASPT2//CASSCF/AMBER, was used to compute the constrained minimum energy profiles (MEPs) along the physically motivated reaction coordinates to model all possible photoisomerization and proton transfer processes. The combination of structural and spectroscopy information will be quantitatively obtained from these high-level QM/MM calculations, which will be used to elucidate the photocycle of PYP.

Computational methods

The structure of PYP in the wild type form was initially obtained from the RCSB protein data bank (PDB) under the code name 3PHY, [61] where the incorporated *p*CA chromophore bears negative charge and has a *trans* configuration. Six Na^+ counter ions and 1046 water molecules were added using the AMBER package.[62] A cutoff radius of 9Å was used for the real space portion of the electrostatic interactions and the van der Waals term, and the AMBER force field parameters for the chromophores were reset using the Gaff module in the AMBER package.[62] Then the system was equilibrated for 1 ns under ambient condition at 298K (NVT ensemble) using the program package TINKER.[63] A cluster analysis of the sampled snapshots generates the appropriate starting structures with strong intermolecular hydrogen bonds for the QM/MM calculation.

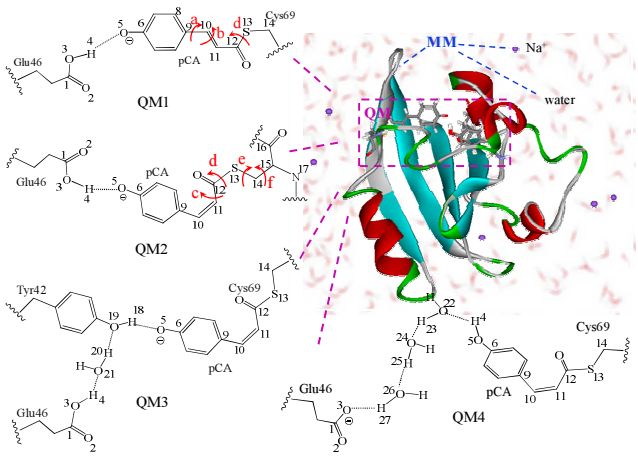

Scheme 1. Illustration of the QM/MM computational protocol adopted in this work. QM1: *p*CA + a portion of the Glu46 and Cys69 residues; QM2: *p*CA + a portion of the Glu46 residue + the Cys69 residue; QM3: *p*CA + a portion of the Glu46, Cys69, Tyr42 residue + one crystal water molecule; QM4: *p*CA + a portion of the residue Glu46, Cys69 + three crystal water molecules. The red arrows indicate the mode of torsional deformation along a(C9-C10), b(C10=C11), c(C11-C12), d(C12-S13), e(S13-C14), and f(C14-C15) bonds, which are defined by the "reaction coordinate" of C8C9C10C11(a), C9C10C11C12(b), C10C11C12S13(c), C11C12S13C14(d), C12S13C14C15(e), S13C14C15C16(f) dihedral angles, respectively

Scheme 1 shows the QM/MM computational protocol adopted in this work. The QM subsystem includes the *p*CA chromophore and its adjacent residues (complete or partial) as well as the crystal water molecules. The remaining residues, water molecules, and counterions were treated by MM. To account for various steps in the photocycle of PYP, different QM/MM partitions were adopted, which gave four types of QM subsystems. As illustrated in scheme 1, QM1 includes the *p*CA chromophore and a portion of the Glu46 and Cys69 residues (33 atoms) for describing the first step of photo-isomerization. Since the later isomerization steps $I_{CP} \rightarrow pR_2$ and $pR_1 \rightarrow pR_2$, as well as subsequent processes, involve two typical structural deformations via the simultaneous torsion along non-adjacent or adjacent two bonds (d/f or d/e), the QM2 subsystem includes the whole Cys69 residue with 40 atoms. To compute the MEPs of the protonation/deprotonation steps, additional one and three crystal water molecules have been added

to the QM3 and QM4 subsystems, respectively. Moreover, part of Tyr42 was also cast into the QM3 subsystem to account for its role of proton transfer relay. Consequently, the numbers of atoms of QM3 and QM4 increase to 52 and 42 from that of 33 in QM1.

CASSCF and CASPT2 methods were used to treat the QM part. The calculations were performed using the GAUSSIAN[64] and MOLCAS[65] program packages. For the MM part AMBER force field was employed using the TINKER tool package. The MOLCAS implementation for the QM/MM interface[66] was employed. A hydrogen link-atom scheme was used to saturate the valence of the QM subsystem, where the bonds between the QM and MM regions were cleaved (indicated by the wavy lines in Scheme 1). To reduce the strong interaction between a link atom and the closest MM point charges, the latter were set to zero.[66] As a compensation some point charges of the MM atoms were re-parameterized as summarized in Table S1 of supporting information (SI).

The local minima in the ground and excited states were obtained by unconstrained CASSCF/AMBER QM/MM optimizations. The constrained minimum energy profiles (MEPs) for the isomerization and proton transfer reactions were computed by stepwise optimizations at the CASSCF level of theory with a 14e/11o active space and 6-31G* basis set. A two-root (S_0, S_1) state-averaged CASSCF procedure with equal weights was employed for the S_1 ($^1\pi\pi^*$) state photo-isomerization calculation and a single root CASSCF optimization was employed for the ground state MEP computation. For each MEP point, a pre-selected reaction coordinate was fixed while the other degrees of freedom were relaxed. This physically motivated reaction coordinate was defined by the angular change for the isomerization and the donor/acceptor distance change for the proton transfer reaction (see Scheme 1), respectively. To describe proton transfer at the ground state, the corresponding donor σ/σ* orbitals and the acceptor n orbital were included in the active space. The rest of 10e/9o came from the high-lying occupied π and low-lying π* orbitals that are mainly distributed in the phenoxy ring of *p*CA. The vertical excitation energies, the corresponding oscillator strengths, and the transition dipole moments for the three lowest excited states of *p*CA in the protein environment were obtained using the ground state CASSCF(14e/11o) optimizations followed by the four-root state-averaged CASPT2 and CASSCF state interaction (CASSI) calculations.

Results and discussion

Photoisomerization at $S_1(^1\pi\pi^*)$ followed by the ground state HT/BP isomerization to pR_1 and I_{CP}.

The $S_0 \rightarrow S_1(^1\pi\pi^*)$ transition of PYP is its lowest lying excitation with a relatively large oscillator strength, f =1.06 (see Table S4-1 in the SI.) The calculated vertical excitation energy is 66.4 kcal/mol (ca. 431 nm), which is consistent with the experimental maximum absorption band of 446 nm.[4,17-18] According to the population analysis this is a typical $\pi \rightarrow \pi^*$ charge transfer excitation where electron migrates from the phenoxy ring to the central double bond C10=C11 (b). This agrees with the previous assignment for the bright state transition of PYP chromophore.[6,67] Consistently, the calculated dipole moment increases from S_0 (equivalent to pG) to $S_1(^1\pi\pi^*)$. This photo-induced charge transfer significantly weakens the C10=C11(b) bond, as indicated by the change in bond length from 1.356 Å in S_0 to 1.443 Å at the minimum of $S_1(^1\pi\pi^*)$ (S_1-Min, equivalent to pG^*). Meanwhile, the H4⋯O5 hydrogen bond length is slightly elongated. These electronic and structural changes facilitate the subsequent isomerization reaction along the C10=C11(b) bond rather than the protonation of the *p*CA chromophore in the $S_1(^1\pi\pi^*)$ excited state.

As expected, the one bond flip photoisomerization in the $S_1(^1\pi\pi^*)$ state of PYP proceeds smoothly along the C10=C11 (b) bond rotary deformation (i.e., the C9C10C11C12 dihedral angle), which has been schematically displayed in the left panel of Figure 2. The initial structural changes in $S_1(^1\pi\pi^*)$ lead to a rapid decay to S_1-Min. Although a fluorescence emission (nanosecond timescale) is possible from here, it cannot compete with the subsequent ultrafast decay for the rotary photo-isomerization along a downhill relaxation pathway. This is why very low fluorescence quantum yield ($\Phi=10^{-3}$) was observed for PYP[12] and *p*CA in gas phase and in solution.[68-70] The calculated wavelength of vertical emission (511 nm) is consistent with the experimentally measured value at 495 nm.[12]

Although the H4⋯O5 hydrogen bond is somewhat weakened during the S_1-FC→S_1-Min decay, the Glu46 residue still serves as a noticeable constraint to the phenoxy ring rotation along the C8C9C10C11 bond in the $S_1(^1\pi\pi^*)$ excited state. Therefore, the photo-isomerization in the $S_1(^1\pi\pi^*)$ state proceeds as one bond flip via the C10=C11(b) bond twist instead of a hula-twist motion through a simultaneous rotation of both the C9C10C11C12 (b) and C8C9C10C11 (a) dihedral angles. As shown in the left panel of Figure 2, with the C10=C11 (b) bond twist the energy of the ground state gradually increases while that of $S_1(^1\pi\pi^*)$ continuously decreases. Consequently, these two states join in the conical intersection region at 85.0° C9C10C11C12 dihedral angle, referred to as CI(S_1/S_0). Meanwhile the carbonyl group undergoes a 21° twist in the C10C11C12O12 dihedral angle from the Frank-Condon point to CI(S_1/S_0). This is consistent with Hache et al's ultrafast time-resolved circular dichroism spectroscopy experiment where a 17-53° carbonyl group twist was observed for the excited state relaxation (<< 0.8 ps).[71] Further increase of the C9C10C11C12 dihedral angle after CI(S_1/S_0) results in a significant increase of the $S_1(^1\pi\pi^*)$ energy, thus ruling out the possibility of a continuous one bond flip photo-isomerization from this critical point. This is mainly due to the strong intermolecular repulsion between the highly strained *p*CA and the protein surrounding (especially from residue Met 100.)

The CI(S_1/S_0) region also serves as an effective nonadiabatic funnel for the alternative $S_1(^1\pi\pi^*) \rightarrow S_0$ deactivation. There are two competing relaxation pathways. The first path leads to the pG recovery, where PYP decays to the ground state *trans* intermediate at 105° C9C10C11C12 dihedral angle (referred to as I_T'). After overcoming a small barrier (4.5 kcal/mol), the system rapidly restores to S_0(pG). This completes a short photo cycle, which is labeled as S_0 (pG) → S_1-Min (pG*) → CI(S_1/S_0) → I_T' → S_0 (pG). Similar mechanism has been proposed that includes a combination of vibrational and conformational relaxation of the chromophore (rather than the protein surrounding) via the *trans* ground state intermediate, which has a 3−6 ps timescale depending on different spectroscopy analyses.[18, 20, 71-72]

Due to the prohibitive computational cost, the above approximate conical intersection region CI(S_1/S_0) was found along the MEPs of preselected reaction coordinates instead of a global optimization. These reaction coordinates are: (i) the simultaneous rotation of the C9C10C11C12 (b) and C8C9C10C11 (a) dihedral angles [Figure 2 (I)]; and (ii) the concerted rotation of b (C9C10C11C12) and d (C11C12S13C14) bonds [Figure 2 (II)]. Similar structures were found in each case for this approximate CI(S_1/S_0) configuration. This suggests that a CI(S_1/S_0) intermediate does exist and participate in the initial stage of the ground state relaxation. The calculated C9C10C11C12 dihedral angle for this approximate CI(S_1/S_0) is 80.0°, which is quite different from those in S_1-Min(155.5°) and S_0 minimum (170.3°) but very close to the experimental value of 85.0° for the first intermediate I_T with a twisted structure using the time-resolved X-ray crystallography technique.[21] Moreover, other geometry parameters of CI(S_1/S_0) are also in good agreement with those of the experimental observation for I_T,[21] which has been summarized in Table 1. Therefore, we still denote the first CI(S_1/S_0)-like intermediate as I_T. There are small differences between the geometries of I_T generated from the hula-twist and the bicycle-pedal isomerization pathways. This indicates that I_T may be a mixture of several intermediates, which has been implied in the previous experimental work.[21]

For the relaxation of pG* → I_T through CI(S_1/S_0), charge transfer takes place along the opposite direction to that of the S_0 → S_1($^1\pi\pi^*$) excitation, i.e., from the central double bond to the phenoxy moiety. This shrinks the phenoxy ring by shortening the C9-C10 bond [1.432 (pG*)→1.360 Å (I_T)] and weakening the intermolecular hydrogen bond [1.752 (pG*)→1.942 Å (I_T)] and the C12-S13 bond [1.793 (pG*)→1.834 Å (I_T)]. Consequently, the constraint on the rotation of the phenoxy ring is largely removed, allowing a volume-conserving hula-twist (HT) isomerization to occur along the simultaneous rotation of the C8C9C10C11 (a) and C9C10C11C12 (b) dihedral angles as shown in Figure 2 (I). Meanwhile, the weakened C12-S13 bond allows another volume-conserving bicycle-pedal (BP) isomerization via the concerted rotation of b (C9C10C11C12) and d (C11C12S13C14) bonds [see Figure 2 (II)]. Overall, the early stage of the PYP photocycle is characterized by a fast photoisomerization, a downhill relaxation to the first ground state twisted intermediate I_T via the CI(S_1/S_0) funnel, and a bifurcation into the subsequent HT and BP isomerization deactivation channels. This highly effective photoisomerization mechanism is consistent with the femto- to pico-second timescale observed for the early-stage intermediate in the experiments.[8,17-18,20-21]

The rearrangement of the hydrogen bonding network also facilitates the subsequent HT and BP isomerizations in the binding pocket composed of various residues (Figure S3-1). The most significant change in the relaxation process is the hydrogen bond between carbonyl C12=O12 in *p*CA and the Met100 residue, i.e., 3.640 Å [S_0(pG)] → 3.910 Å [S_1-Min(pG*)] → 3.140 Å [CI(S_1/S_0)] → 3.400 Å (I_T). The strengthened hydrogen bond from pG* to CI(S_1/S_0) is caused by the C10=C11 bond rotary photoisomerization, which accounts for the energy increase in the S_1($^1\pi\pi^*$) state relaxation. The weakened hydrogen bond during the CI(S_1/S_0)→I_T decay allows a further isomerization associated

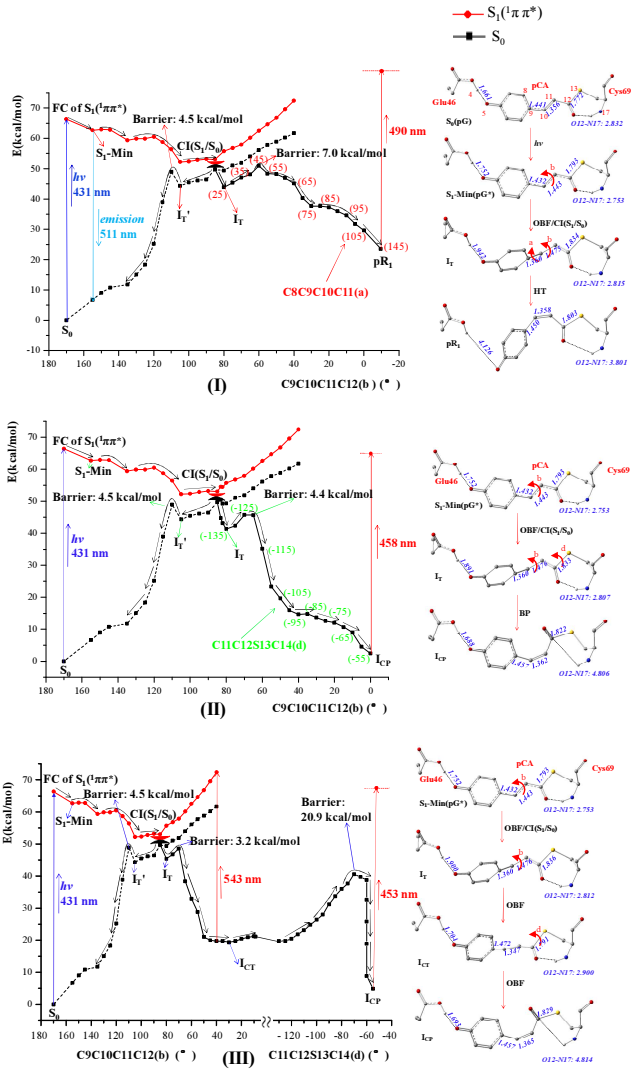

Figure 2. MEPs of the one-bond flip (OBF) photoisomerization in the S_1($^1\pi\pi^*$) state of PYP along b bond rotation that is defined by the C9C10C11C12(b) dihedral angle, followed by three different ground state isomerization pathways: (I) simultaneous a, b bonds hula-twist (HT); (II) concerted b, d bonds bicycle-pedal (BP); and (III) OBF motion alone b or d. The values of the C8C9C10C11 (a) dihedral angle are in red while C11C12S13C14 (d) are in green, respectively. The related isomerization barriers are also highlighted.

with C12=O12 twist in the ground state. Consequently, both the HT and BP ground state isomerizations proceed smoothly with moderate barriers (7.0 and 4.4 kcal/mol). Compared with the BP isomerization, the HT rotary deformation is slightly more difficult since a relatively larger phenoxy ring twist is involved with the breaking of the *p*CA-Glu46 inter-residue hydrogen bond [O5-H4 distance 1.942 Å (I_T) → 4.126 Å (pR_1)], in which a pair of adjacent double (b) and single (a) bonds flanking a single C10-H10 unit rotate concertedly.

In contrast, the phenoxy ring remains unchanged in the BP isomerization, producing an intermediate I_{CP} with a *cis* planar-like structure [Figure 2 (II)]. Simultaneous rotations occur along the two nonadjacent bonds (b and d), with cleavage of the *p*CA-Cys69 inter-residue hydrogen bond [O12-H17 distance 1.839 Å (I_T) → 4.406 Å (I_{CP})]. Consistent with the recent time-resolved

X-ray crystallography experiment,[21] the HT isomerization of I_T can compete with the BP rotary deformation in the wild type PYP since they have similar barriers. The BP pathway can be switched off completely by weakening the hydrogen bond between the phenolate ring and the adjacent residue through the E46Q mutation, which makes the HT rotary deformation the only relaxation channel. This reveals the important role of hydrogen bonding network for isomerization reactions in protein.[21]

Table 1. Comparison of the geometry parameters for the ground state intermediates of the *p*CA chromophore between the calculated (this work) and experimental values [ref 21 and ref 25(I_{CP}).]

		pG	I_T	I_{CP}	I_{CT}	pR_1	pR_2
O5-Glu46	Cal.	2.65	2.85	2.67	--	5.02	2.78
(O5-O3, Å)	Exp.	2.60	2.80	2.70	3.30	5.40	3.40
O12-Cys69	Cal.	2.83	2.81	4.88	--	3.80	3.20
(O12-N17, Å)	Exp.	2.80	2.90	4.90	4.70	3.30	4.10
C9C10C11C12(°)	Cal.	170.0	80.0	-3.6	--	-6.7	14.2
	Exp.	169.0	85.0	-2.0	-1.0	1.0	3.0
C8C9C10C11(°)	Cal.	-3.6	21.9	14.4	--	145.3	13.6
	Exp.	-8.3	15.1	8.2	47.6	149.9	21.1
C10C11C12O12(°)	Cal.	-9.0	16.5	-3.1	--	12.7	14.5
	Exp.	-8.3	16.6	-2.7	-4.5	-17.1	15.6

Overcoming two moderate barriers, the HT and BP isomerizations produce two different *cis* isomers pR_1 and I_{CP} along downhill reaction pathways. The vertical excitation energy of the $S_0 \rightarrow S_1$ transition for pR_1 is 490 nm, which is 59 nm red shifted with respect to that of the *trans* isomer pG $\rightarrow S_1$. This agrees with the experimental results.[26,28,32,33,34] As illustrated in Figure 2 (I) and (II), the main structural difference between pR_1 and I_{CP} is the orientation of the carbonyl group C12=O12, which respectively lies on the same or opposite side of the pG chromophore. Moreover, there are some differences in the way how the hydrogen bonds break during isomerization. The loss of the *p*CA-Glu46 inter-residue hydrogen bond leads to a minor twist of the phenolate ring in pR_1, where the C9C10C11C12 , C8C9C10C11 and C10C11C12O12 dihedral angles display non-planar values in both theory and experiment[21] (see Table 1). Conversely, the retention of the *p*CA-Glu46 inter-residue hydrogen bond in I_{CP} facilitates a quasi-coplanar arrangement. The C8C9C10C11 dihedral angle of I_{CP} is 14.4° in this work, which is close to the value of 8.2° for the *cis* planar-like intermediate identified in earlier work[25] but differs from 47.6° in the recent assignment of the I_{CT} intermediate along the BP isomerization pathway.[21] Our calculation reveals that I_{CP} is 21.1 kcal/mol more stable than pR_1 and is only 2.4 kcal/mol higher than pG (S_0), which reflects the role of the *p*CA-Glu46 inter-residue hydrogen bond in energy stabilization. I_{CP} leads to another red-shifted intermediate (458 nm) with small energy difference (4.0 kcal/mol) compared with the vertical excitation of pG (S_0) → S1.

Besides the above concerted pathways, the stepwise isomerization mechanism was also examined in Figure 2 (III). It first proceeds through one bond flip rotation of C9C10C11C12 (b) same as the photoisomerization in the $S_1(^1\pi\pi^*)$ state, leading to an energy plateau. Both the C8C9C10C11 and C10C11C12O12 dihedral angles are found to undergo further twist along this plateau. This twisted arrangement maintains the *p*CA-Glu46 inter-residue hydrogen bond as identified by the picosecond X-ray crystallography.[21] It results in a significant increase in the energy of the I_{CT} intermediate. Consequently, its vertical excitation to S_1 shows a noticeable red shift compared with that of pG(S_0) → S_1, producing an absorption band longer than 500 nm. The calculation agrees with the experimental observation where a red-shifted absorption peak at 510 nm was found for an early intermediate in the PYP photocycle.[17] Although this initial one bond flip rotation takes place easily due to the small (3.2 kcal/mol) barrier, the stepwise mechanism is less favorable because of a higher barrier (20.9 kcal/mol) has to be overcome in the second step when rotating along the C11C12S13C14 (d) angle.

Overall, the CI(S_1/S_0) region serves as the first branching point for the excited state relaxation to the complete and short photocycle through the intermediates I_T [resembling CI(S_1/S_0)] and I_T' [resembling pG(S_0)], respectively. This explains the 0.5 quantum yield of the ground state repopulation that was observed experimentally in the "unsuccessful" photocycle pathways.[18,20] Two major and one minor deactivation channels were found starting from the CI(S_1/S_0)-like intermediate I_T, producing the *cis* isomers pR_1, I_{CP}, and I_{CT} through a hula twist, a bicycle pedal and a one bond flip isomerization reaction, respectively.

The assignment of the intermediates has been controversial for the multi-step PYP photo-cycle.[73-74] Recently, Anfinrud et al performed density functional theory (DFT) QM/MM calculations[73] and raised doubt on the earliest intermediate I_T proposed experimentally by Ihee et. al.[21] They found a much flatter (21°) I_T intermediate[73] that differs significantly from the 79°/81° central dihedral angle found in Ihee et. al's X-ray structures.[21] In contrast, the present CASPT2//CASSCF/Amber QM/MM computation supports the highly strained I_T intermediate (80°) measured by Ihee et. al. As discussed above, I_T originates from the nonadiabatic $S_1 \rightarrow S_0$ relaxation through the CI(S_1/S_0) conical intersection and naturally exhibits structural resemblance to CI(S_1/S_0). Furthermore, it is widely accepted that CI(S_1/S_0) locates halfway between the *trans*- and *cis*-isomers with a ~90° torsional angle. Therefore, the 80° angle is a reasonable value. The ultrafast $S_1 \rightarrow S_0$ relaxation can be completed within a few picoseconds, which accounts for the persistence of I_T in the ~2 ps excited state lifetime of PYP[75].

In the experimental studies two early-stage intermediates I_0 and $I^{\ddagger}_0$ were identified, where I_0 is formed within less than 3 ps and decays on a time scale of ~220 ps to $I^{\ddagger}_0$, which in turn decays on a time scale of 3.0 ns to pR.[17, 18, 76-78] This assigned I_0 is roughly equivalent to I_T in this work because of the barrierless characteristic in forming I_T through the process S_0 (pG) → S_1-Min (pG*) → CI(S_1/S_0) → I_T. Considering that moderate barriers have to be overcome in the bicycle pedal/hula twist isomerization pathways, another intermediate $I^{\ddagger}_0$ corresponds to a mixture of pR_1 and I_{CP}, which is slightly different from the experimental assignment[21] (pR_1 and I_{CT}). Compared with the measured longer timescales, the calculated barriers (4.4-7.0 kcal/mol) overestimate the rate for generating the pR_1 and I_{CT} intermediates. This is due to the significant conformational entropy change in the protein surrounding for the *trans* → *cis* *p*CA chromophore bicycle pedal/hula twist isomerization. On the other hand, there is no drastic entropy change in the short photocycle of S_0(pG) → S_1-Min(pG*) → CI(S_1/S_0) → I_T' → S_0(pG) via the *trans* ground state

intermediate, where the calculated barrier (4.5 kcal/mol) is consistent with the 3−6 ps timescale measured in experiment.[18,71-72]

BP isomerization from I_{CP} to pR_2 followed by the protonation reaction producing pB'.

As shown in Figure 3, a simultaneous rotation around the C12-S13 and C14-C15 bonds is an effective isomerization pathway for the I_{CP} to pR_2 transition. As expected, pR_2 is generated through this bicycle pedal rotation where the C11C12S13C14 dihedral angle changes from the *syn* (-55˚) in I_{CP} to the *anti* (-175˚) structure in pR_2. A large barrier (16.2 kcal/mol) in the pathway explains the long timescale (16-21 ns) observed experimentally[21, 25, 79] for the I_{CP}→pR_2 transition. The barrier is mainly due to the distorted C12=O12 carbonyl group in the protein cavity. The structure gradually recovers to a quasi-planar arrangement after the barrier, followed by a downhill energy profile to the final product pR_2. The *p*CA-Cys69 (O12-H17: 4.253→2.468 Å) and *p*CA-Phe96 (S13-H: 3.520→2.894 Å) intermolecular hydrogen bonds are significantly strengthened from I_{CP} to pR_2, resulting in 10.0 kcal/mol decrease in energy. A similar stabilization energy (7.0 kcal/mol) for the I_{CP}→pR_2 transition was estimated in a previous DFT calculation.[79] The vertical excitation energy of S_0 →S_1 transition for the red-shifted intermediate pR_2 is calculated to be 61.1 kcal/mol (468 nm), which agrees well with the experimental value of 460-465 nm.[22,30, 32, 80]

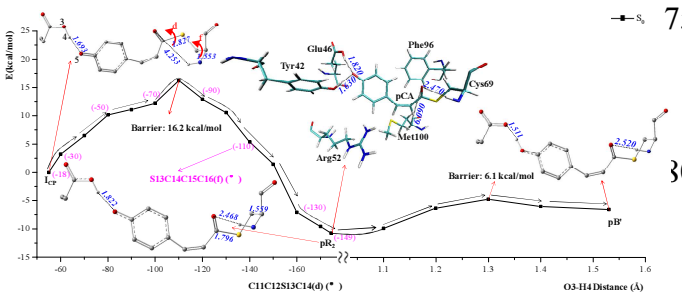

Figure 3. MEPs of the BP isomerization from I_{CP} to pR_2 through a simultaneous rotation of the C11C12S13C14(d) and S13C14C15C16 (f) dihedral angles, followed by the intermolecular proton transfer between *p*CA and Glu46 producing pB' along the RC of O3-H4 distance. The values of the S13C14C15C16 (f) dihedral angle are shown in red. The related barriers are also highlighted.

Apart from the above structural changes, charge transfer from the thioester bond to the phenolate ring is found during the I_{CP}→ pR_2 relaxation. Consequently, negative charge is accumulated around O5 of the phenoxy ring, which can function as an acceptor for the subsequent protonation reaction. A 6.1 kcal/mol barrier is encountered when proton H4 moves from O3 of Glu46 towards O5, producing the protonated state of *p*CA, hereafter referred to as pB'. Such a low barrier hydrogen bond (LBHB) transition between Glu46 and PYP has been discussed in previous experimental[40] and theoretical studies.[81] The proton transfer does not introduce any drastic structural changes in *p*CA, and it proceeds within a short time. Since the fast protonation reaction pR_2→pB' follows the slow bicycle pedal isomerization I_{CP}→pR_2 (16-21 ns), the dynamics and structural spectroscopy of pB' overlaps with that of pR_2. This inevitably leads to some ambiguities in the structure and timescale assignments among different experimental and theoretical studies.[32-33,34,36]

The blue-shifted intermediate pB' is 4.25 kcal/mol less stable than pR_2 due to the new negative charge center, the COO^- group. The calculated absorption wavelength is 356 nm, very close to the experimental value of 355-360 nm.[33, 36] Consistent with the previous experimental observations,[32-34] the COO^- group of Glu46 is still buried in the binding pocket (Figure S3-1). Thus, pB' is in hydrophobic form and tends to undergo further structural changes to expose the buried COO^- group of Glu46 to the water solvent.

Hydrophobic-hydrophilic state transformation of pB'→pB followed by the deprotonation reaction and S_0(pG) recovery.

Experimentally, a large conformational change was proposed in the transition of the blue-shifted intermediate pB' to pB.[32-34] However, there is no detailed information on how this takes place and whether the *p*CA chromophore is involved in the process. By comparing experimental crystal structures[25] of pB' and pB with many sample computations, we found that a bicycle pedal isomerization is required along the simultaneous rotation of the two nonadjacent single bonds (c and e), followed by a reverse one-bond flip deformation along the C11-C12 (c) bond. As shown in Figure 4 (I), from pB' energy gradually increases to the maximum at -80.0˚ C10C11C12S13 and -10.0˚ C12S13C14C15 dihedral angles along the bicycle pedal isomerization pathway. A 26.6 kcal/mol barrier exists in this process, followed by a stable intermediate where an intermolecular hydrogen bond is formed between *p*CA and Cys69. The relative position between C12=O12 and the S atom in the intermediate is inverted comparing with that in pB', but is the same as that in S_0(pG). This supports that the bicycle pedal isomerization is a step to approach the S_0(pG) recovery.

In the second step the *p*CA chromophore undergoes a reverse one-bond flip isomerization along the C11-C12 (c) bond to achieve the overall pB'→ intermediate→ pB transition. The C10C11C12S13 angle varies as -170˚(pB') → -30˚(intermediate) → -170˚(pB) in a bicycle pedal then a one-bond flip isomerization. The 80.2˚ phenolate ring twist causes a 28.4 kcal/mol raise in energy. Meanwhile, the intermolecular hydrogen bond between *p*CA and Glu46 (O3-H4 distance) increases from 1.511 Å in pB' to 7.437 Å in pB. This exposes the buried COO- group of Glu46 to the water solvent, transforming the hydrophobic pB' to the precursor state of hydrophilic pB. A large-amplitude protein conformational change coordinates the hydrophobic-hydrophilic pB'→pB transition. Due to the significant entropy and energy change, the pB'→pB transition occurs very slowly, as also confirmed by the 2 ms timescale measured experimentally.[33-34]

The exposed COO^- group of Glu46 serves as a proton acceptor and attracts water solvent into the binding pocket. Three water molecules form a water wire between the COO^- group of Glu46 and the hydroxyl group of *p*CA, in preparation for the subsequent deprotonation reaction [Figure 4 (II)]. The formation of the hydrophilic state decreases the energy by more than 20 kcal/mol. This hydrogen bond stabilization energy is in good agreement with the previous experimental[82] and theoretical[83] estimates.

The deprotonation reaction then proceeds smoothly through two steps of proton migration. The COO^- group first overcomes a

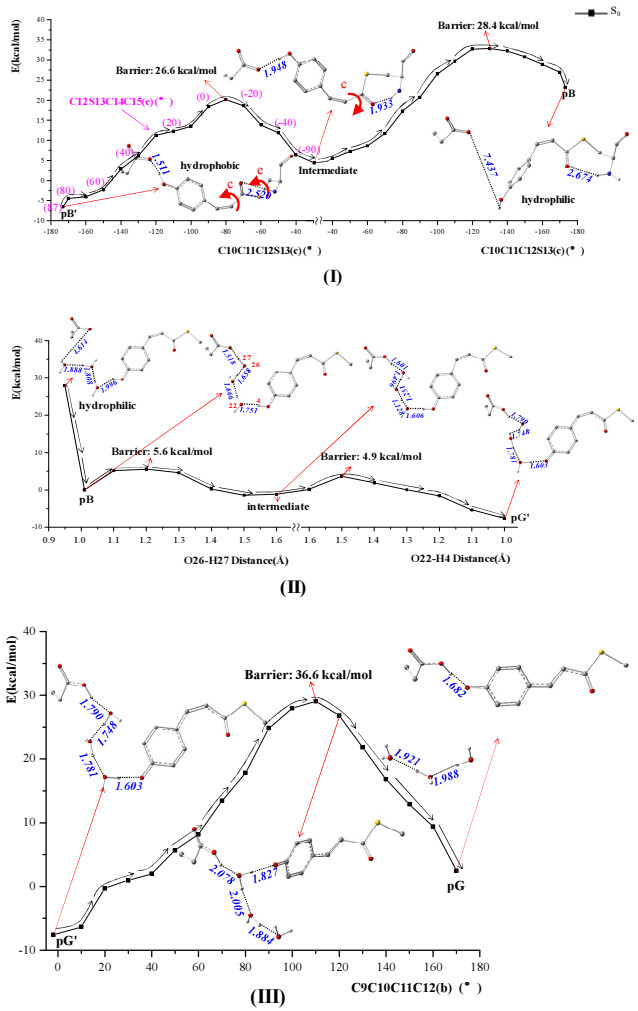

Figure 4. MEPs of the BP and reverse OBF isomerizations for pB'→pB transition through (I) the simultaneous rotation of both C10C11C12S13(c)/C12S13C14C15 (e) and alone C10C11C12S13(c) dihedral angles, and followed (II) deprotonation reaction producing pG' along the RC of O26-H27 and O22-H4 distances (Å) as well as (III) OBF isomerization of pG'→pG transition along RC of C9C10C11C12(b) dihedral angle. The values (in degree) of the C12S13C14C15 (e) dihedral angle are shown in red and the related barriers are also highlighted.

5.6 kcal/mol barrier to receive one proton from the water wire, relaxing to an intermediate. The hydroxyl group of the *p*CA chromophore then overcomes a 4.9 kcal/mol barrier to donate the proton to a neighboring water, producing pG' and completes the deprotonation reaction. As discussed above, this low-barrier proton transfer without large-amplitude protein motion unlikely participates in the slow relaxation of the isomerization cycle.

Up to now, all groups of the *p*CA chromophore but the phenoxy ring have returned to their S_0(pG) arrangement. The S_0(pG) recovery of the phenoxy ring is achieved through a one-bond flip isomerization along the C10=C11 (b) double bond as shown in Figure 4 (III). The isomerization is difficult due to the double bond constraint and the fact that two hydrogen bonds among the COO^- group of Glu46/water wire/phenoxy ring of the *p*CA chromophore have to be broken. A 30~40 kcal/mol barrier is found at 110° C9C10C11C12 dihedral angle. Consistently, a very long time scale (ms-s) for this transition was measured experimentally.[25-26] The breaking of the two hydrogen bonds and the phenoxy ring rotation repels water molecules out of the binding package, regenerates the hydrogen bond between Glu46 and *p*CA, and finally completes PYP photocycle.

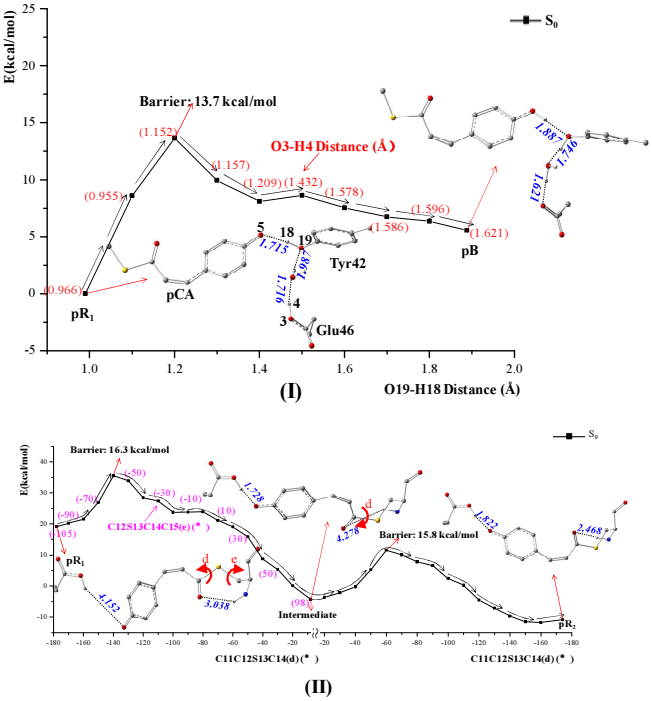

Figure 5. (I) MEPs of pR_1→pB through concerted proton transfer along the reaction coordinates of O19-H18 and O3-H4 distances; (II) MEPs of HT and reverse OBF isomerizations for the pR_1→pR_2 transition through a simultaneous rotation of the C11C12S13C14(d) and C12S13C14C15(e) dihedral angles, and alone the C11C12S13C14(d) dihedral angle. The values of the O3-H4 distance and the C12S13C14C15 (e) dihedral angle) are shown in red. The related barriers are also highlighted.

Parallel versus sequential pathways through competitive pR_1→pB and pR_1→pR_2 transitions.

The kinetics of the parallel and sequential reactions is determined by two competing channels: pR_1→pB and pR_1→pR_2 (Figure 5). As mentioned above, pR_1 and pB exhibit structural resemblance in chromophore orientation (the hydrophilic precursor state) and the surrounding hydrogen bond environment (the broken *p*CA-Glu46 inter-residue hydrogen bond). The major structural difference is that *p*CA is in the deprotonation state in pR_1 whereas Glu46 is deprotonated in pB. This change is achieved by the protonation reaction of *p*CA in pR_1 assisted by the proton transfer relay of the nearby Tyr42 residue and water molecule. As shown in Figure 5(I), the inter-residue hydrogen bond between *p*CA and Tyr42 (O5-H18) is shortened to 1.715 Å during the departure of Glu46 upon the pR_1 formation. This initiates the proton transfer from the hydroxyl group of Tyr42 to

the phenoxy group of *p*CA. However, the C=O group of *p*CA is not a good proton acceptor at the pR_1 state since there is no obvious accumulation of negative charge around the O atom. Thus, energy increases sharply when proton H18 moves from Tyr42 to *p*CA. During the process H4 of Glu46 simultaneously moves towards the bridging water, which induces a proton approaching O19 of Tyr42. Along this concerted pathway, the protonation reaction for *p*CA occurs over a sizeable barrier (13.7 kcal/mol) and producing the protonated *p*CA chromophore (pB).

Although pR_1 is ~30 kcal/mol more stable than pR_2, the $pR_1 \rightarrow pR_2$ transition is difficult since a spatial inversion between the S atom and the C12=O12 group and an inter-residue hydrogen bond recovery between *p*CA and Glu46 are required to take place. Similar to the pB' → pB transition [Figure 4(I)], pR_1 first undergoes a hula twist isomerization via a simultaneous rotation of the C11C12S13C14(d) and C12S13C14C15(e) dihedral angles and then via a reverse one-bond flip isomerization along the C11C12S13C14(d) dihedral angle from -10 to -180°. As shown in Figure 5 (II), a 16.3 kcal/mol barrier exists in the first step due to the strong intermolecular repulsion between a highly strained *p*CA and the protein surrounding. Similarly, a barrier of 15.8 kcal/mol was found in the hydrogen bond recovery pathway where a highly strained *p*CA was formed again. After passing those two barriers, the inter-residue hydrogen bond between pCA and Glu46 is recovered to complete the $pR_1 \rightarrow pR_2$ transition along a downhill pathway. Similar to $pR_1 \rightarrow pB$, the $pR_1 \rightarrow pR_2$ transition is a high barrier process, which is consistent with the microsecond time scale found in the experiment[25,27,29] for both the $pR_1 \rightarrow pR_2$ and $pR_1 \rightarrow pB$ transitions. The present computational result suggests that the parallel process through the $pR_1 \rightarrow pB$ transition is a favorable channel but coexists with the sequential pathway via the $pR_1 \rightarrow pR_2$ transition. The two processes have similar barriers in the rate-determining step (13.7 vs 16.3 kal/mol).

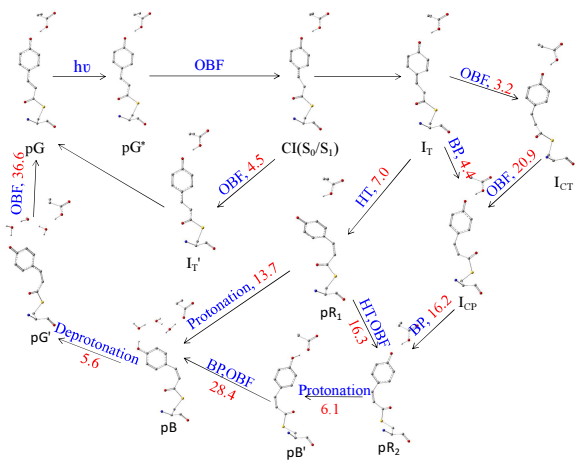

Scheme 2: Mechanistic illustration of the overall PYP photocycle: the protonation/deprotonation and isomerization reactions of the hula twist (HT), bicycle pedal (BP) and one-bond flip (OBF) are shown in red along the special one or two bonds (letter in parentheses) and the related barriers (kcal/mol) are also highlighted in blue.

Conclusions

In this work a CASPT2//CASSCF/AMBER QM/MM approach was employed to investigate the isomerization and protonation reactions upon the photoexcitation of the wild-type PYP. The study provides a comprehensive picture for the overall photocycle, as illustrated in Scheme 2. The conical intersection $CI(S_1/S_0)$ plays a critical role to bifurcate the excited state relaxation to the complete and short photocycles through different intermediates, I_T [$CI(S_1/S_0)$ like] and I_T' [$pG(S_0)$ like]. Two major and one minor deactivation channels were found starting from the $CI(S_1/S_0)$-like intermediate I_T, producing the *cis* isomers pR_1, I_{CP}, and I_{CT} through the hula twist, bicycle pedal and one-bond flip isomerization reactions. The $I_{CP} \rightarrow pB'$ transition is achieved by a high-barrier bicycle pedal isomerization and a fast protonation reaction of the *p*CA chromophore through a red-shifted intermediate pR_2. Another high-barrier bicycle pedal isomerization followed by a reverse one bond flip isomerization leads to a hydrophobic-hydrophilic transformation and the formation of a high energy state pB, leaving a considerable space between *p*CA and Glu46. This allows the exposed COO^- group of Glu46 to attract water solvent into the binding pocket through the slit between the surrounding protein residues and thus further triggers the fast deprotonation reaction of *p*CA. The photocycle is finally completed by the ground state recovery of the phenoxy ring repelling water molecules out of the binding pocket through a one bond flip isomerization with a large barrier. Analysis unveils that parallel mechanism through $pR_1 \rightarrow pB$ transition is a favorable channel but coexists with the sequential model via the $pR_1 \rightarrow pR_2$ transformation.

Acknowledgements

This work was supported by the NCET-11-0030 and NSFC21373029 (X.C.), NSFC21033002 and Major State Basic Research Development Programs 2011CB808503 (W.F.), and the National Science Foundation CHE-1012479 (H.W.).

Notes and references

[a] *Key Laboratory of Theoretical and Computational Photochemistry of Ministry of Education, Department of Chemistry, Beijing Normal University, Xin-wai-da-jie No. 19, Beijing, 100875, China, Emails: xuebochen@bnu.edu.cn*

[b] *Department of Chemistry and Biochemistry, New Mexico State University, Las Cruces, NM 88003, USA, Email: haobin@nmsu.edu*

†Electronic Supplementary Information (ESI) available: Figures and Tables as well as Cartesian coordinates. See DOI:10.1039/b000000x/

References

1 T. E, Meyer, *Biochim. Biophys. Acta.*, 1985, **806**, 175-183.

2 R. Kort, W. D. Hoff, M. Van West, A. R. Kroon, S. M. Hoffer, K. Vlieg, W. Crielaard, J. J. Van Beeumen, K. J. Hellingwerf, *Embo. J.*, 1996, **15**, 3209–3218.

3 J. L. Pellequer, K. A. Wager-Smith, S. A. Kay, E. D. Getzoff, *Proc. Natl. Acad. Sci. U.S.A.*, 1998, **95**, 5884-5890.

4 M. A. Cusanovich, T. E. Meyer, *Biochem.*, 2003, **42**, 4759-4770.

5 B. Perman, V. Šrajer, Z. Ren, T. Teng, C. Pradervand, T. Ursby, D. Bourgeois, F. Schotte, M. Wulff, R. Kort, K. Hellingwerf, K. Moffat, *Science*, 1998, **279**, 1946-1950.

6 E. V. Gromov, I. Burghardt, H. Köppel, L. S. Cederbaum, *J. Am. Chem. Soc*., 2007, **129**, 6798-6806.
7 W. W. Sprenger, W. D. Hoff, J. P. Armitage, K. J. Hellingwerf, *J. Bacteriol*., 1993, **175**, 3096–3104.
8 M. L. Groot, L. J. G. W. van Wilderen, D. S. Larsen, M. A. van der Horst, I. H. M. van Stokkum, K. J. Hellingwerf, R. van Grondelle, *Biochemistry*, 2003, **42**, 10054-10059.
9 T. Gensch, K. J. Hellingwerf, S. E. Braslavsky, K. Schaffner, *Phys. Chem. A*, 1998, **102**, 5398-5405.
10 M. E. Van Brederode, T. Gensch, W. D. Hoff, K. J. Hellingwerf, S. E. Braslavsky, *Biophys. J*., 1995, **68**, 1101-1109.
11 S. Devanathan, S. Lin, M. A. Cusanovich, N. Woodbury, G. Tollin, *Biophys. J*., 2000, **79**, 2132–2137.
12 T. E. Meyer, G. Tollin, T. P. Causgrove, P. Cheng, R. E. Blankenship, *Biophys. J*., 1991, **59**, 988-991.
13 Y. Hori, H. Ueno, S. Mizukami, K. Kikuchi, *J. Am. Chem. Soc*., 2009, **131**, 16610–16611.
14 Y. Hori, K. Nakaki, M. Sato, S. Mizukami, K. Kikuchi, *Angew. Chem. Int. Ed. Engl*., 2012, **51**, 5611-5614.
15 Y. Hori, T. Norinobu, M. Sato, K. Arita, M. Shirakawa, K. Kikuchi, *J. Am. Chem. Soc*., 2013, **135**, 12360−12365.
16 Y. Hori, K. Kikuchi, *Curr. Opin. Chem. Biol*., 2013, **17**, 644–650.
17 L. Ujj, S. Devanathan, T. E. Meyer, M. A. Cusanovich, G. Tollin, G. H. Atkinson,*Biophys. J*., 1998, **75**, 406-412.
18 S. Devanathan, A. Pacheco, L. Ujj, M. Cusanovich, G. Tollin, S. Lin, N. Woodbury, *Biophys. J*., 1999, **77**, 1017–1023.
19 T. Gensch, C. C. Gradinaru, I. H. M. van Stokkum, J. Hendriks, K. J. Hellingwerf, R. van Grondelle, *Chem. Phys. Lett*., 2002, **356**, 347–354.
20 K. Heyne, O. F. Mohammed, A. Usman, J. Dreyer, E. T. J. Nibbering, M. A. Cusanovich, *J. Am. Chem. Soc*., 2005, **127**, 18100-18106.
21 Y. O. Jung, J. H. Lee, J. Kim, M. Schmidt, K. Moffat, V. Šrajer, H. Ihee, *Nat. Chem*., 2013, **5**, 212-220.
22 R. Brudler, R. Rammelsberg, T. T. Woo, E. D. Getzoff, K. Gerwert, *Nat. Struct. Bio*., 2001, **8**, 265-270.
23 M. Unno, M. Kumauchi, N. Hamada, F. Tokunaga, S. Yamauchi, *J. Biol. Chem*., 2004, **279**, 23855–23858.
24 Y. Imamoto, M. Kataoka, F. Tokunaga, T. Asahi, H. Masuhara, *Biochemistry*, 2001, **40**, 6047–6052.
25 H. Ihee, S. Rajagopal, V. Šrajer, R. Pahl, S. Anderson, M. Schmidt, F. Schotte, P. A. Anfinrud, M. Wulff, K. Moffat, *Proc. Natl. Acad. Sci. U.S.A*., 2005, **102**, 7145–7150.
26 T. W. Kim, J. H. Lee, J. Choi, K. H. Kim, L. J. van Wilderen, L. Guerin, Y. Kim, Y. O. Jung, C. Yang, J. Kim, M. Wulff, J. J. van Thor, H. Ihee, *J. Am. Chem. Soc*., 2012, **134**, 3145–3153.
27 K. Takeshita, Y. Imamoto, M. Kataoka, K. Mihara, F. Tokunaga, M. Terazima, *Biophys. J*., 2002, **83**, 1567–1577.
28 A. Losi, T. Gensch, M. A. van der Horst, K. J. Hellingwerf, S. E. Braslavsky, *Phys. Chem. Chem. Phys*., 2005, **7**, 2229-2236.
29 Y. Hoshihara, Y. Imamoto, M. Kataoka, F. Tokunaga, M. Terazima, *Biophys. J*., 2008, **94**, 2187–2193.
30 S. Yeremenko, I. H. M. van Stokkum, K. Moffat, K. J. Hellingwerf, *Biophys. J*., 2006, **90**, 4224–4235.
31 P. Khoroshyy, A. Dér, L. Zimányi, *J. Photochem. Photobiol. B*, 2013, **120**, 111–119.
32 A. Xie, W. D. Hoff, A. R. Kroon, K. J. Hellingwerf, *Biochemistry*, 1996, **35**, 14671-14678.
33 A. Xie, L. Kelemen, J. Hendriks, B. J. White, K. J. Hellingwerf, W. D. Hoff, *Biochemistry*, 2001, **40**, 1510-1517.
34 D. Pan, A. Philip, W. D. Hoff, R. A. Mathies, *Biophys. J*., 2004, **86**, 2374-2382.
35 N. Shimizu, Y. Imamoto, M. Harigai, H. Kamikubo, Y. Yamazaki, M. Kataoka, *J. Biol. Chem*., 2006, **281**, 4318–4325..
36 J. Hendriks, I. H. M. van Stokkum, K. J. Hellingwerf, *Biophys. J*., 2003, **84**, 1180–1191.
37 J. Hendriks, K. J. Hellingwerf, *J. Biol. Chem*., 2009, **284**, 5277–5288.
38 G. E. O. Borgstahl, D. R. Williams, E. D. Getzoff, *Biochemistry*, 1995, **34**, 6278-6287.
39 R. Kort, K. J. Hellingwerf, R. B. G. Ravelli, *J. Biol. Chem*., 2004, **279**, 26417–26424.
40 S. Yamaguchi, H. Kamikubo, K. Kurihara, R. Kuroki, N. Niimura, N. Shimizu, Y. Yamazaki, M. Kataoka, *Proc. Natl. Acad. Sci. U.S.A*., 2009, **106**, 440-444.
41 S. Tripathi, V. Srajer, N. Purwar, R. Henning, M. Schmidt, *Biophys. J*., 2012, **102**, 325-332.
42 Y-W. Hsiao, W. Thiel, *J. Phys. Chem. B*, 2011, **115**, 2097–2106.
43 J. Vreede, J. Juraszek, P. G. Bolhuis, *Proc. Natl. Acad. Sci. U.S.A*., 2010, **107**, 2397–2402.
44 J. Hendriks, W. D. Hoff, W. Crielaard, K. J. Hellingwerf, *J. Biol. Chem*., 1999, **274**, 17655–17660.
45 K. J. Hellingwerf, J. Hendriks, T. Gensch, *J. Phys. Chem. A*, 2003, **107**, 1082-1094.
46 D. S. Larsen, R. van Grondelle, *ChemPhysChem*, 2005, **6**, 828–837.
47 B. Borucki, S. Devanathan, H. Otto, M. A. Cusanovich, G. Tollin, M. P. Heyn, *Biochemistry*, 2002, **41**, 10026-10037.
48 B. G. Levine, T. Martínez, *J. Ann. Rev. Phys. Chem*., 2007, **58**, 613-634.
49 S. R. Meech, *Chem. Soc. Rev*., 2009, **38**, 2922-2934.
50 M. J. Thompson, D. Bashford, L. Noodleman, E. D. Getzoff, *J. Am. Chem. Soc*., 2003, **125**, 8186-8194.
51 C. Ko, B. Levine, A. Toniolo, L. Manohar, S. Olsen, H. J. Werner, T. J. Martínez, *J. Am. Chem. Soc*., 2003, **125**, 12710-12711.
52 M. Boggio-Pasqua, C. F. Burmeister, M. A. Robb, G. Groenhof, *Phys. Chem. Chem. Phys*., 2012, **14**, 7912–7928.
53 E. V. Gromov, I. Burghardt, H. Köppel, L. S. Cederbaum, *J. Phys. Chem. A*, 2011, **115**, 9237–9248.
54 C. M. Isborn, B. D. Mar, B. F. E Curchod, I. Tavernelli, T. J. Martínez, *J. Phys. Chem. B*, 2013, 117, 12189−12201.
55 G. Groenhof, M. F. Lensink, H. J. C. Berendsen, J. G. Snijders, A. E. Mark, *Proteins: Struct., Funct., Genet*., 2002, **48**, 202–211.
56 G. Groenhof, M. F. Lensink, H. J. C. Berendsen, A. E. Mark, *Proteins: Struct., Funct., Genet*., 2002, **48**, 212–219.
57 G. Groenhof, M. Bouxin-Cademartory, B. Hess, S. P. de Visser, H. J. C. Berendsen, M. Olivucci, A. E. Mark, M. A. Robb, *J. Am. Chem. Soc*., 2004, **126**, 4228-4233.
58 I. Antes, W. Thiel, W. F. van Gunsteren, *Eur. Biophys. J*., 2002, **31**, 504–520.
59 E. J. M. Leenders, L. Guidoni, U. Röthlisberger, J. Vreede, P. G. Bolhuis, E. J. Meijer, *J. Phys. Chem. B*, 2007, **111**, 3765-3773.
60 C. M. Isborn, A. W. Götz, M. A. Clark, R. C. Walker, T. J. Martínez, *J. Chem. Theory Comput*., 2012, **8**, 5092–5106.
61 P. Düx, G. Rubinstenn, G. W. Vuister, R. Boelens, F. A. A. Mulder, K. Hård, W. D. Hoff, A. R. Kroon, W. Crielaard, K. J. Hellingwerf, R. Kaptein, *Biochemistry*, 1998, **37**, 12689-12699.
62 D. A. Case, T. A. Darden, T. E. Cheatham III, C. L. Simmerling, J. Wang, R. E. Duke, R. Luo, K. M. Merz, D. A. Pearlman, M. Crowley, R. C. Walker, W. Zhang, B. Wang, S. Hayik, A. Roitberg, G. Seabra, K. F. Wong, F. Paesani, X. Wu, S. Brozell, V. Tsui, H. Gohlke, L. Yang, C. Tan, J. Mongan, V. Hornak, G. Cui, P. Beroza, D. H. Mathews, C. Schafmeister, W.S. Ross, P. A. Kollman, AMBER 9, University of California, San Francisco, 2006.
63 J. W. Ponder, F. M. Richards, *J. Comput. Chem*., 1987, **8**, 1016-1024.
64 Gaussian 03, Revision D.02, M. J. Frisch, G. W. Trucks, H. B. Schlegel, G. E. Scuseria, M. A. Robb, J. R. Cheeseman, J. A. Montgomery, Jr., T. Vreven, K. N. Kudin, J. C. Burant, J. M. Millam, S. S. Iyengar, J. Tomasi, V. Barone, B. Mennucci, M. Cossi, G. Scalmani, N. Rega, G. A. Petersson, H. Nakatsuji, M. Hada, M. Ehara, K. Toyota, R. Fukuda, J. Hasegawa, M. Ishida, T. Nakajima, Y. Honda, O. Kitao, H. Nakai, M. Klene, X. Li, J. E. Knox, H. P. Hratchian, J. B. Cross, V. Bakken, C. Adamo, J. Jaramillo, R. Gomperts, R. E. Stratmann, O. Yazyev, A. J. Austin, R. Cammi, C. Pomelli, J. W. Ochterski, P. Y. Ayala, K. Morokuma, G. A. Voth, P. Salvador, J. J. Dannenberg, V. G. Zakrzewski, S. Dapprich, A. D. Daniels, M. C. Strain, O. Farkas, D. K. Malick, A. D. Rabuck, K. Raghavachari, J. B. Foresman, J. V. Ortiz, Q. Cui, A. G. Baboul, S. Clifford, J. Cioslowski, B. B. Stefanov, G. Liu, A. Liashenko, P. Piskorz, I. Komaromi, R. L. Martin, D. J. Fox, T. Keith, M. A. Al-Laham, C. Y. Peng, A. Nanayakkara, M. Challacombe, P. M. W. Gill, B. Johnson, W. Chen, M. W. Wong, C. Gonzalez and J. A. Pople, Gaussian, Inc., Wallingford CT, 2004.

65 G. Karlström, R. Lindh, P.-Å. Malmqvist, B. O. Roos, U. Ryde, V. Veryazov, P.-O. Widmark, M. Cossi, B. Schimmelpfennig, P. Neogrady, L. Seijo, *Comput. Mater. Sci*., 2003, **28**, 222-239.
66 N. Ferré, A. Cembran, M. Garavelli, M. Olivucci, *Theo. Chem. Acc.*, 2004, **112**, 335-341.
67 P. B. Coto, S. Martí, M. Oliva, M. Olivucci, M. Merchán, J. Andrés, *J. Phys. Chem. B*, 2008, **112**, 7153–7156.
68 A. Espagne, D. H. Paik, P. Changenet-Barret, P. Plaza, M. M. Martin, A. H. Zewail, *Photochem. Photobiol. Sci*., 2007, **6**, 780–787.
69 W. L. Ryan, D. J. Gordon, D. H. Levy, *J. Am. Chem. Soc*., 2002, **124**, 6194-6201.
70 M. Putschögl, P. Zirak, A. Penzkofer, *Chem. Phys*. 2008, **343**, 107–120.
71 L. Mendonça, F. Hache, P. Changenet-Barret, P. Plaza, H. Chosrowjan, S. Taniguchi, Y. Imamoto, *J. Am. Chem. Soc*., 2013, **135**, 14637−14643.
72 P. Changenet-Barret, P. Plaza, M. M. Martin, H. Chosrowjan, S. Taniguchi, N. Mataga, Y. Imamoto, M. Kataoka, *J. Phys. Chem. C*, 2009, **113**, 11605-11613.
73 V. R. I. Kaila, F. Schotte, H. S. Cho, G. Hummer, P. A. Anfinrud, *Nat. Chem*., 2014, **6**, 258-259.
74 Y. O. Jung, J. H. Lee, J. Kim, M. Schmidt, K. Moffa, V. Šrajer, H. Ihee, *Nat. Chem*., 2014, **6**, 259-260.
75 D. S. Larsen, I. H. M. van Stokkum, M. Vengris, M. A. van der Horst, F. L. de Weerd, K. J. Hellingwerf, R. van Grondelle, *Biophys. J*., 2004, **87**, 1858-1872.
76 L. J. G. M. Wilderen, M. A. van der Horst, I. H. M. van Stokkum, K. J. Hellingwerf, R. van Grondelle, M. L. Groot, *Proc. Natl. Acad. Sci. U.S.A*., 2006, **103**, 15050–15055.
77 Y. Imamoto, Y. Shirahige, F. Tokunaga, T. Kinoshita, K. Yoshihara, M. Kataoka, *Biochemistry*, 2001, **40**, 8997–9004
78 Z. Ren, K. Moffat, *J. Appl. Crystallog*r., 1995, **28**, 461–481.
79 F, Schotte, H. S. Cho, V. R. I. Kaila, H. Kamikubo, N. Dashdorj, E. R. Henry, T. J. Graber, R. Henning, M. Wulff, G. Hummer, M. Kataoka, P. A. Anfinrud, *Proc. Natl. Acad. Sci. U.S.A*., 2012, **109**, 19256-19261.
80 T. E. Meyer, E. Yakali, M. A. Cusanovich, G. Tollin, *Biochemistry*, 1987, **26**, 418-423.
81 M. Nadal-Ferret, R. Gelabert, M. Moreno, J. M. Lluch, *J. Am. Chem. Soc*., 2014, **136**, 3542-3552.
82 V. Brenner, F. Piuzzi, I. Dimicoli, B. Tardivel, M. Mons, *Angew. Chem. Int. Ed*., 2007, **46**, 2463-2466.
83 X. B. Chen, L. H. Gao, W. H. Fang, D. L. Phillips, *J. Phys.Chem. B*, 2010, **114**, 5206−5214.

Graphical abstract

A comprehensive picture for the overall photocycle was obtained to reveal a wide range of structural signaling in photoactive yellow protein.